Room temperature phosphorescence from natural wood activated by external chloride anion treatment

Yingxiang Zhai[1], Shujun Li [1 ✉], Jian Li[1], Shouxin Liu[1], Tony D. James [2,3 ✉], Jonathan L. Sessler [4 ✉] & Zhijun Chen [1 ✉]

Producing afterglow room temperature phosphorescence (RTP) from natural sources is an attractive approach to sustainable RTP materials. However, converting natural resources to RTP materials often requires toxic reagents or complex processing. Here we report that natural wood may be converted into a viable RTP material by treating with magnesium chloride. Specifically, immersing natural wood into an aqueous $MgCl_2$ solution at room temperature produces so-called C-wood containing chloride anions that act to promote spin orbit coupling (SOC) and increase the RTP lifetime. Produced in this manner, C-wood exhibits an intense RTP emission with a lifetime of ~ 297 ms (vs. the ca. 17.5 ms seen for natural wood). As a demonstration of potential utility, an afterglow wood sculpture is prepared in situ by simply spraying the original sculpture with a $MgCl_2$ solution. C-wood was also mixed with polypropylene (PP) to generate printable afterglow fibers suitable for the fabrication of luminescent plastics via 3D printing. We anticipate that the present study will facilitate the development of sustainable RTP materials.

Afterglow room temperature phosphorescence (RTP) emission is defined as emission lasting for more than 100 ms after removal of the excitation source[1]. Materials with afterglow RTP emission exhibit long lifetimes, large Stokes shifts, and good signal-to-noise ratios. Often, they can be visualized readily by the naked eye. These attributes have made RTP materials attractive for use in a wide variety of applications, including visual decorations, optical sensing, biological imaging, and information encryption[2–6]. Organic afterglow RTP materials derived from natural sources are of particular interest since they are expected to be sustainable, flexible, biocompatible, and available at scale[7,8].

To obtain sustainable afterglow RTP materials, two crucial barriers must be overcome[9–11]. First, the triplet excitons of the chromophores inherent in the source material must be effectively populated by facilitating ISC from singlet excitons to triplet excitons, which typically requires efficient spin-orbit coupling (SOC)[12,13]. Second,

nonradiative deactivation of the resulting triplet excitons must be suppressed[14–18].

Guided by these principles, two general strategies for fabricating effective sustainable afterglow RTP materials have been pursued. The first approach relies on converting biomass materials (such as, gelatin, cellulose and rice husks) to carbon dots endowed with efficient SOC; these dots are then confined in an organic matrix to stabilize the triplet excitons[19–21]. Another strategy involves using directly untreated natural materials, such as lignin, gelatin and cellulose, as chromophores incorporated within a rigid matrix[22–25]. However, the fabrication of these sustainable RTP systems generally involves the use of toxic reagents, energy-consuming processes, or complex procedures that are difficult to carry out on large scale. For example, from our previous research we converted wood to structural RTP materials using lignin oxidation assisted by NaOH and concentrated H_2O_2[25]. However, drying

the concentrated H_2O_2-incoporated wood in the oven at high temperatures is very dangerous (potentially explosive). Also, oxidation of lignin destroys the physicochemical stability of the wood[26–29]. As a result, there remains a need for methods that allow afterglow RTP materials to be prepared conveniently and cost-effectively from sustainable sources.

To address the above challenge, we were drawn to wood. Wood is a largely renewable resource that exhibits short phosphorescence (~17–30 ms), a result attributed to the confinement of lignin within the associated cellulose and hemicellulose matrix[25,30,31]. Previous reports have indicated that the lifetime of phosphorescent chromophores can be enhanced by treating with heavy atom salts[32–34], certain small molecules[35–39] or polymers[40–42]. However, these approaches have not been extensively exploited for the creation of natural wood-based afterglow RTP materials in a mild manner. As detailed below, we have now successfully enhanced the lifetime of natural wood from ~17.5 ms to ~297 ms by treating with 1 M aqueous magnesium chloride for 2 sec at room temperature (Fig. 1a). The as-obtained chloride ion-containing wood (C-wood) exhibited ultra-long afterglow emission. With a view toward preparing C-wood rapidly and reproducibly (Fig. 1b), we developed an automatic manufacturing line wherein the source wood was manipulated by robots and subject to immersion in an aqueous $MgCl_2$ solution before being placed on the line for transportation and drying (Fig. 1c and Supplementary Movie 1). We also found that C-wood could be converted to afterglow fibers using polypropylene (PP), thus allowing its use in 3D printing.

Generally, natural wood was converted to RTP materials (C-wood) with a lifetime of ~297 ms assisted by external chloride ions. As-prepared C-wood showed great potential as luminescent materials for 3D printing.

Results

Afterglow RTP emission of C-wood

In this study, basswood was chosen as a representative natural wood. It was converted to C-wood by soaking in 1 mol L^{-1} (M) aqueous $MgCl_2$ for

Fig. 1 | Preparation of C-wood. a Schematic showing the preparation of room temperature phosphorescent C-wood from natural basswood. **b** Photographs of C-wood under bright field (upper), UV irradiation (middle), and after switching off the UV light (bottom). Afterglow images were acquired at 120 ms after switching off the UV light. **c** Cartoon illustration of an automatic production line for converting natural wood into an afterglow material.

2 s at room temperature. The $MgCl_2$ loading of C-wood is 8.5%, determined by changes in mass. An automatic manufacturing line was also developed for preparing the wood in a convenient and rapid manner (Supplementary Movie 1). SEM imaging studies confirmed that the resulting C-wood maintained a porous structure analogous to that of the original source wood (Fig. 2a and Supplementary Fig. 1). Elemental mapping of the C-wood confirmed that C, O, Mg and Cl are evenly distributed within the wood cell walls (Fig. 2b). Moreover, the XRD pattern for the C-wood produced in this way exhibited the characteristic signals of natural wood and $MgCl_2$, leading us to conclude that treatment with $MgCl_2$ did not alter the basic structure of the source material (Fig. 2c). Specifically, the natural wood exhibited a strong signal in 20°, which was attributed to Type I cellulose in the wood matrix[43]. Treatment using $MgCl_2$ did not change the crystal structure of the natural wood. Spectroscopic analyses of the C-wood revealed a fluorescence emission feature centered at 465 nm and strong afterglow RTP emission centered at 545 nm with a lifetime of ~ 297 ms and the quantum yield was ~ 4.7% (Fig. 2d to f, Supplementary Fig. 2 and Supplementary Movie 2). To confirm reproducibility, we prepared 5 samples under the same conditions and measured their lifetimes with 5 repeat measurements being made for each sample (Supplementary Fig. 3). Concordant and reproducible results were obtained. In contrast, untreated wood exhibited a weak afterglow emission and a relatively short lifetime (~ 17.5 ms) (Supplementary Fig. 2). Time-resolved spectroscopic[44–46] analyses confirmed that C-wood produces a long-lasting and stable afterglow phosphorescence feature centered at 545 nm following photoexcitation at 365 nm, with this emission remaining detectable for as long as 1100 ms (Fig. 2g). The lifetime of the C-wood could be tuned by varying the concentration of the $MgCl_2$ solution with which the native wood was treated. For instance, the lifetime of C-wood could be increased to ca. 364 ms when 2 M $MgCl_2$ was used (Fig. 2h). Native wood treated in an analogous way with different monovalent, divalent or trivalent chloride anion salts at equivalent chloride anion concentrations (2 M), including $AlCl_3$, $ZnCl_2$, KCl, NaCl, $BaCl_2$, $SrCl_2$ and $CaCl_2$, also exhibited enhanced lifetimes when compared with the untreated wood (control group) (Fig. 2i). To exclude the effect of varied pH of these solution on the RTP emission of wood, natural wood was treated using the corresponding pH mediated by acid (CH_3COOH) or base ($NH_3·H_2O$). The treated wood did not show enhanced RTP lifetime (Supplementary Fig. 4 and Supplementary Fig. 5).

Samples were also prepared by treating natural basswood with $Mg(NO_3)_2$ and $MgSO_4$. Basswood treated with $Mg(NO_3)_2$ (N-wood) and $MgSO_4$ (S-wood) exhibited weak phosphorescence emission and shorter lifetimes of 4.9 ms and 36.6 ms, respectively (Fig. 2j and k). The reduced lifetime of N-wood was proposed to reflect the quenching effect of NO_3 anions[47,48]. We thus conclude that the chloride anion plays a determinative role in enhancing the RTP lifetime. Other halide anion salts, namely KBr, $MgBr_2$, and KI, were also evaluated; again, an enhancement in the RTP lifetime was observed (Supplementary Fig. 6–8). However, for reasons of ease, efficacy, and cost we focused on $MgCl_2$ in the present study.

To verify that the $MgCl_2$ was crucial for RTP emission, C-wood was washed with water to remove the $MgCl_2$. After washing, the lifetime of C-wood decreased from ca. 284 ms to approximately 94 ms with a concomitant decrease in the elemental chlorine content from 3.97% to 0.91%, determined by XPS analysis (Fig. 2l and Supplementary Fig. 9). The effect of environmental humidity on the phosphorescence lifetime of C-wood was also evaluated. The humidity can quench the triplet excitons[49,50]. As a result, the C-wood was easily quenched by humidity. It was found that the phosphorescence lifetime decreased as the humidity increased. For instance, the phosphorescence lifetime dropped to 5.89 ms when the humidity reached 90% (Supplementary Fig. 10). The phosphorescence lifetime recovered after the sample was dried. Only a modest degradation in the RTP lifetime of the dried
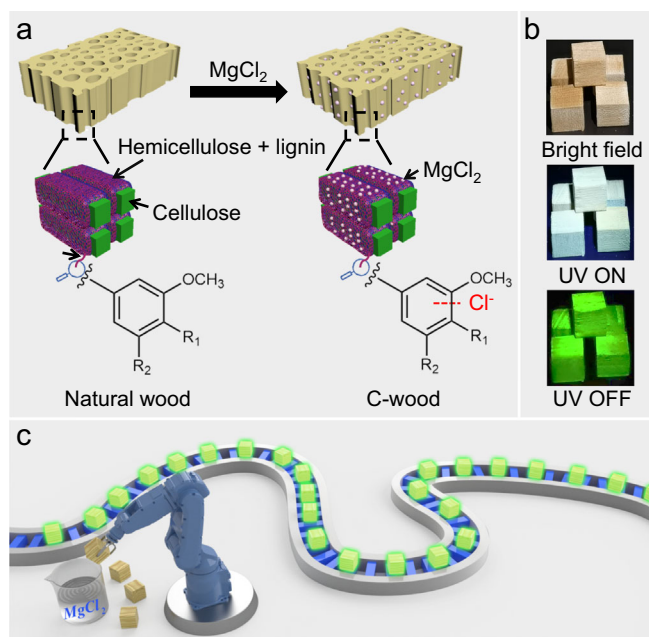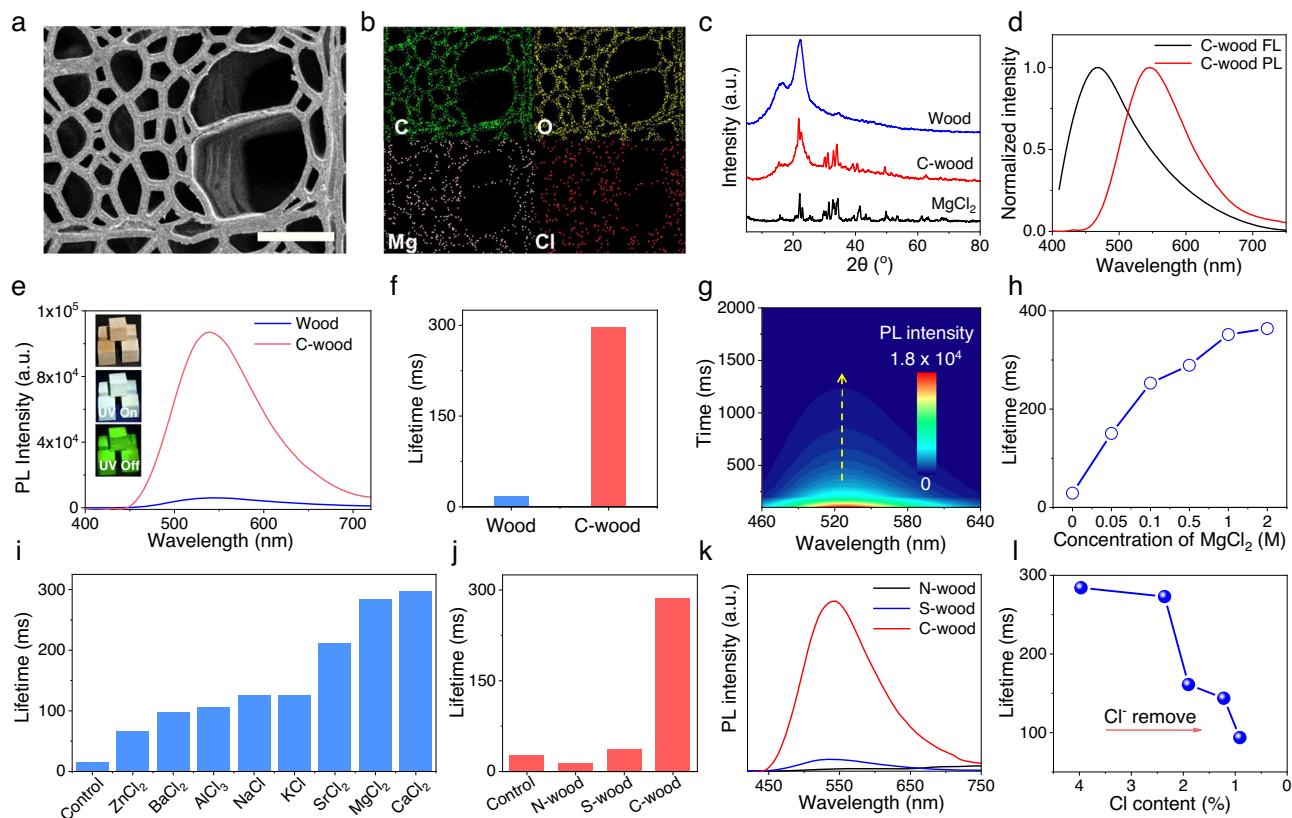
Fig. 2 | RTP emission of C-wood. a Scanning electron microscopy (SEM) images of C-wood; scale bar = 50 μm. **b** Elemental mapping of C-wood: C, O, Mg and Cl. **c** X-ray diffraction (XRD) pattern of wood (blue line), C-wood (red line) and $MgCl_2$ (black line). **d** Fluorescence (FL, black line) and Phosphorescence (PL, red line) spectra of C-wood treated with 1 M aqueous $MgCl_2$ at room temperature. **e**, Phosphorescence spectra of C-wood (red line) and natural wood (blue line) at room temperature. Afterglow images were acquired at 120 ms after switching off the UV light. **f** Lifetime of wood and C-wood. **g** Time-dependent phosphorescence emission of C-wood. **h**, RTP lifetime of C-wood treated with different concentration of $MgCl_2$. **i** Lifetime of C-wood prepared using different salts; the concentration of chloride anions was 2 M in all cases. **j** Lifetime of C-wood (Basswood treated with 1 M $MgCl_2$), S-wood (Basswood treated with 1 M $MgSO_4$) and N-wood (Basswood treated with 1 M $Mg(NO_3)_2$) at room temperature. **k** RTP spectra of C-wood (red line), S-wood (blue line) and N-wood (black line). **l** Effect of Cl content on the C-wood RTP lifetime. Excitation wavelength = 365 nm.

C-wood was observed over the course of repeated "humidifying-dehumidifying" cycles (Supplementary Fig. 11). However, the problem can be solved by coating the RTP wood with a hydrophobic wax. After coating with wood wax, the lifetime of wood did not decrease upon changes of humidity (Supplementary Fig. 12).

Mechanism and universal design

To further understand the role of lignin, delignified wood was prepared[51]. As expected, delignified wood exhibited very short phosphorescence lifetime (~2.1 ms). Introducing $MgCl_2$ to the delignified wood did not obviously enhance its RTP lifetime (~2.3 ms) (Supplementary Fig. 13). Additionally, embedding technical lignin, such as, alkali lignin (AL) and lignin sulfonate (LS-Na) in cellulose pulp resulted in RTP emissions with lifetimes of 127.5 ms and 141.7 ms, respectively. In addition, the value increased to 554.7 ms and 356.1 ms, respectively upon addition of $MgCl_2$ (Supplementary Fig. 14 and Supplementary Fig. 15). All these results confirmed that lignin is the RTP chromophore in the wood matrix and could be activated by external chloride anions.

To gain insights into the determinants underlying the observed increase in the RTP lifetime seen for C-wood, theoretical calculations were performed. Here, a model unit (Supplementary Fig. 16) was employed for lignin-carbohydrate complexes in the wood[52]. As determined by the high-resolution XPS spectral studies, there are two types of Cl⁻ in C-wood, namely Cl⁻ from free $MgCl_2$ and Cl⁻ from coordinated $MgCl_2$[53] (Supplementary Fig. 17). Both types of Cl⁻ anions were considered in the calculations (Fig. 3b). The distance between the Cl⁻ (from

coordinated $MgCl_2$) and the closest π surface was found to vary between 4.6 and 5.0 Å, leading us to conclude that the chloride anion −π interactions are at best modest (Supplementary Fig. 18). However, the corresponding Cl⁻···π distance (for the free $MgCl_2$) proved to be 3.56 Å. This relatively close contact was expected to facilitate SOC promoted by the chloride anion. (Fig. 3b and Supplementary Fig. 18). The theoretical calculations also provided support for the notion that the SOC constant for C-wood (0.30 cm⁻¹) was higher than the value of natural wood (0.11 cm⁻¹), S-wood (0.04 cm⁻¹) and N-wood (0.037 cm⁻¹) (Fig. 3a). A strong SOC facilitates ISC and thus serves to enhance the RTP emission. Spin-orbit coupling values are positively correlated with generation of singlet oxygen[54–56]. Therefore, we determined the generation of singlet oxygen by C-wood and natural wood using 9,10-anthracenediyl-bis(methylene)-dimalonic acid (ABDA) as a singlet oxygen probe[57]. The results indicated that C-wood exhibited a faster and more significant generation of singlet oxygen than natural wood, suggesting that C-wood has an enhanced SOC value (Supplementary Fig. 19). On the bases of these analyses, we propose that it is the Cl⁻···π interactions in the $MgCl_2$-treated samples that give rise to the observed long afterglow emission.

To test whether the present strategy could be expanded to include other types of wood, samples of poplar, teak, maple, balsa, schima, walnut, beech and pine wood were treated with $MgCl_2$ using the same protocol as described above. In all cases, the resulting samples were found to fluorescence blue when irradiated at 365 nm and produce a long-lived yellow-green phosphorescence.
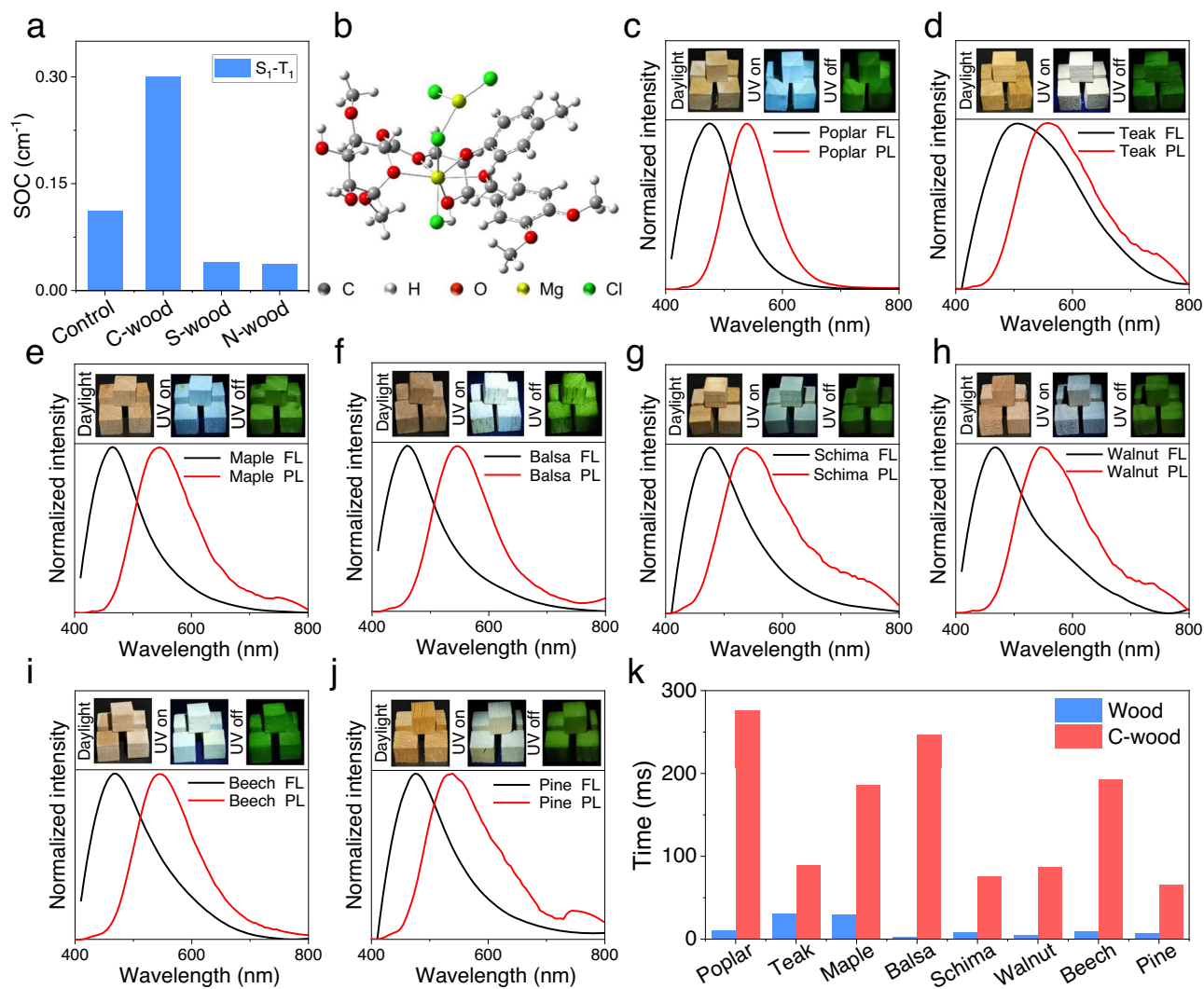
Fig. 3 | Mechanistic studies and tests of generality. a Spin orbit coupling (SOC) values between the S_1 and T_1 states calculated for model C-wood, S-wood, N-wood and Control (natural wood) samples. **b** Simulated structure of a C-wood model. **c–j** Fluorescence (black line) and phosphorescence (red line) spectra of poplar, teak, maple, balsa, schima, walnut, beech and pine treated with 1 M aqueous $MgCl_2$ at room temperature. The inset shows C-wood before (left) and after (right) turning off the excitation source (a 365 nm UV lamp). All afterglow images in **c–j** were acquired at 120 ms after switching off the UV light. **k**, RTP lifetime of poplar, teak, maple, balsa, schima, walnut, beech, pine and the corresponding C-wood forms. Excitation wavelength = 365 nm.

Interestingly, the C-wood made from different types of wood exhibited different emission spectra and lifetimes. To better understand why this was the case, the loading and inherent physiochemical properties of natural wood were analyzed. Mass analysis indicated that the wood had different $MgCl_2$ loading amount although they were treated with the same concentration of $MgCl_2$ solution (Supplementary Fig. 20). This was attributed to different adsorbance capacities of the wood caused by the various porous structures[58–61] (Fig. 4a). Notably, C-wood made from basswood and schima wood displayed different spectra and lifetime although they had similar $MgCl_2$ loading. This was associated with the inherent physiochemical properties of lignin in the wood, which is crucial for the RTP emission. Generally, lignin consists of three aromatic units, guaiacyl lignin (G), syringyl lignin (S) and para-hydroxy-phenyl lignin (H) linked by C-O-C and C-C bond. The ratios of these aromatic units and linkages varies between wood species[62,63]. These different molecular structures, supramolecular aggregates and concentrations of lignin can result in different photoluminescence properties[64,65]. To clarify the difference of lignin in these woods, the content of lignin was characterized using the Klason method[66]. As expected, the content of lignin in these woods was different and varied from 23.2% to 34.4% (Fig. 4c). Also, taking basswood, beech and pine as examples, 2D HSQC NMR analysis was performed[67]. The results indicated that lignin in these woods had different G/S/H ratios and structures (Fig. 4b). All these results suggest that a different loading of $MgCl_2$ and the inherent physiochemical properties of lignin contribute to the various emission spectra and lifetimes.

The corresponding afterglow RTP lifetimes for the treated poplar, teak, maple, balsa, schima, walnut, beech and pine wood samples were 275.87 ms, 89.94 ms, 186.41 ms, 246.10 ms, 76.08 ms, 87.34 ms, 193.04 ms and 66.04 ms, respectively. These RTP effects could be observed easily by the naked eye after the UV lamp was switched off (Fig. 3c-k). We thus suggest that $MgCl_2$ treatment provides a general means of preparing afterglow materials from wood. Additionally, the long-lived RTP lifetime of C-wood using different wood species was also investigated (Fig. 4d, e). The corresponding afterglow RTP lifetimes for the treated poplar, teak, maple, balsa, schima, walnut, beech and pine wood samples were 285.66 ms, 77.21 ms, 289.46 ms, 287.99 ms, 140.82 ms, 174.23 ms, 253.91 ms and 153.13 ms, respectively.
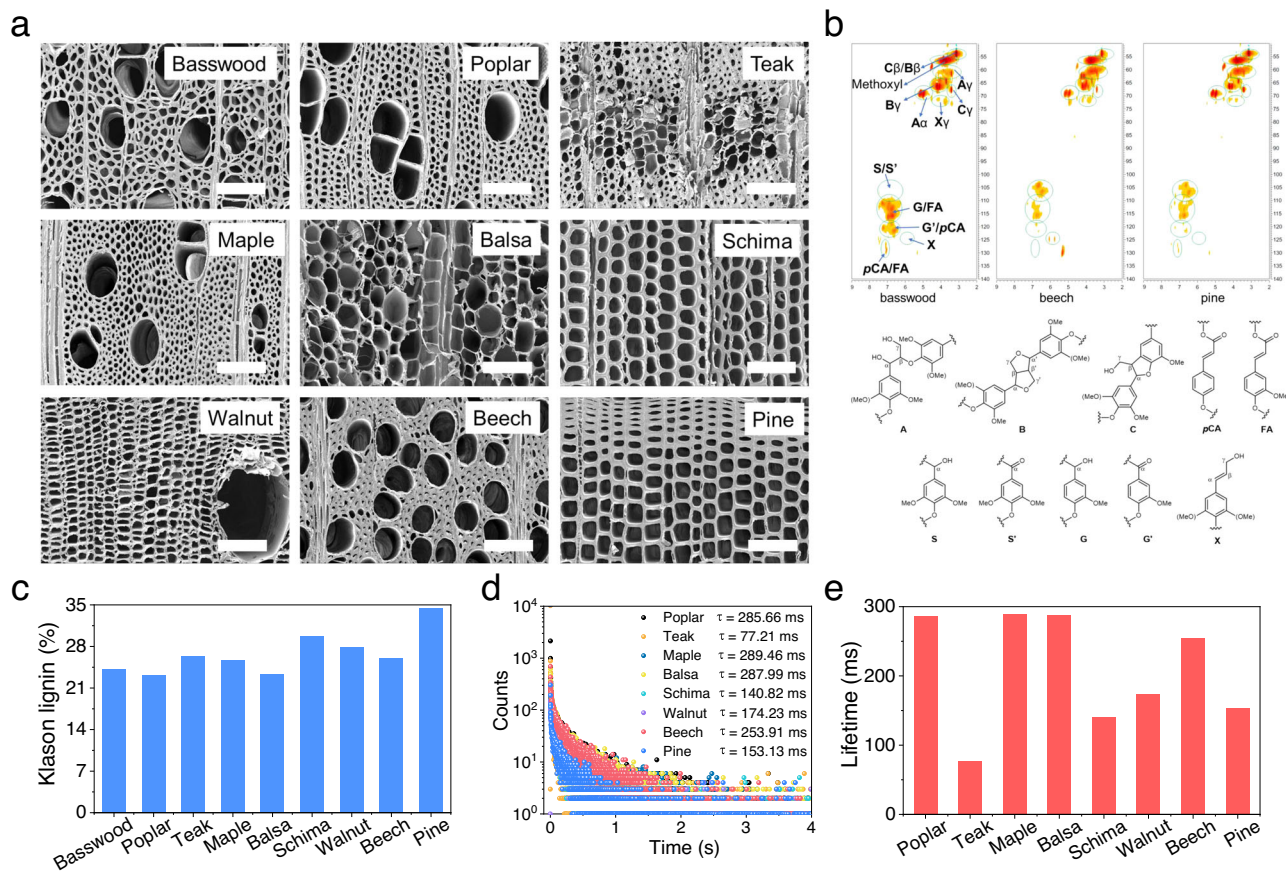
Fig. 4 | Mechanism for different RTP behavior from various wood species. a SEM image of different natural wood, scale bar = 100 μm. **b** The 2D HSQC NMR spectra of lignin from basswood, beech and pine (DMSO-d₆, 200 mg mL⁻¹). **c** Klason lignin content of basswood, poplar, teak, maple, balsa, schima, walnut, beech and pine. RTP decay profiles (**d**) and RTP lifetime (**e**) of poplar, teak, maple, balsa, schima, walnut, beech and pine treated with 1 M CaCl₂. Excitation wavelength = 365 nm.

Potential applications

Sustainable indoor lighting materials represent an obvious and substantial requirement. The present C-wood approach could play a role in this regard. In order to evaluate this possibility, a basswood sculpture was sprayed with a MgCl₂ solution. In accord with our expectations, the treated sculpture exhibited afterglow emission (Fig. 5a). Moreover, patterned structures could be obtained by spraying MgCl₂ through a template onto the surface of a basswood surface (Fig. 5b, c).

Luminescent plastics are another material of interest. They exhibit promise for use in energy-storage applications[68], LED production[69] and information storage[50]. 3D printable luminescent plastics have received particularly attention in this context due to the ever-increasing demand for irregularly shaped materials. To test whether the present C-wood could be used to prepare afterglow luminescent plastics useful for 3D printing, we mixed C-wood with polypropylene (PP). Specifically, C-wood powder (10 g) was mixed with PP (990 g) to provide C-wood/PP bulk composites (cf. Supporting Information for experimental details). Subsequently the C-wood/PP bulk composite was processed to generate printable fibers using a screw extruder (Fig. 5d, e). The fibers exhibited a tensile strengthen of 25.63 Mpa (Supplementary Fig. 21). These fibers were then printed into representative shapes, such as a rabbit, honeycomb, and pinecone, (Fig. 5f). All the resulting constructs exhibited long afterglow emission following photoexcitation. Moreover, the printed sample did not show any lifetime decrease after storage for 3 months (Supplementary Fig. 22).

Discussion

In summary, we have demonstrated that natural woods may be converted into afterglow RTP materials by simply treating with aqueous MgCl₂. The lifetime of natural basswood could be increased by ~17-fold (to give an RTP lifetime of ~ 297 ms) by treating with aqueous 1 M MgCl₂ for 2 sec at room temperature. This increase is ascribed to the enhancement in SOC produced by the embedded chloride anions. In operational terms, it is important to note that no significant energy-consuming steps or toxic reagents were required for the conversion of native wood to C-wood. Further, C-wood in combination with PP could be employed to produce afterglow printable fibers, which could then be 3D printed to create a variety of RTP constructs. We believe our materials exhibit many advantages for practical applications, when compared with traditional RTP materials: a. The raw sources used for the RTP materials were sustainable and renewable wood, which could be obtained in a large scale at a low price, b. The method of fabricating the RTP materials from natural wood was simple and mild and does not generate toxic byproducts during the preparation; c. Additionally, our wood-derived RTP materials could be easily converted to powders, films and structural materials suitable for any practical applications[25,70]. Considering these benefits, we believe that the present strategy could find use in a range of application areas where RTP materials might prove useful, including in anti-counterfeiting operations, flexible display production, and generation of textiles and luminescent coatings. Research into C-wood remains in its infancy and as such shortcomings associated with practical applications exist, particularly when compared with other emerging phosphorescent
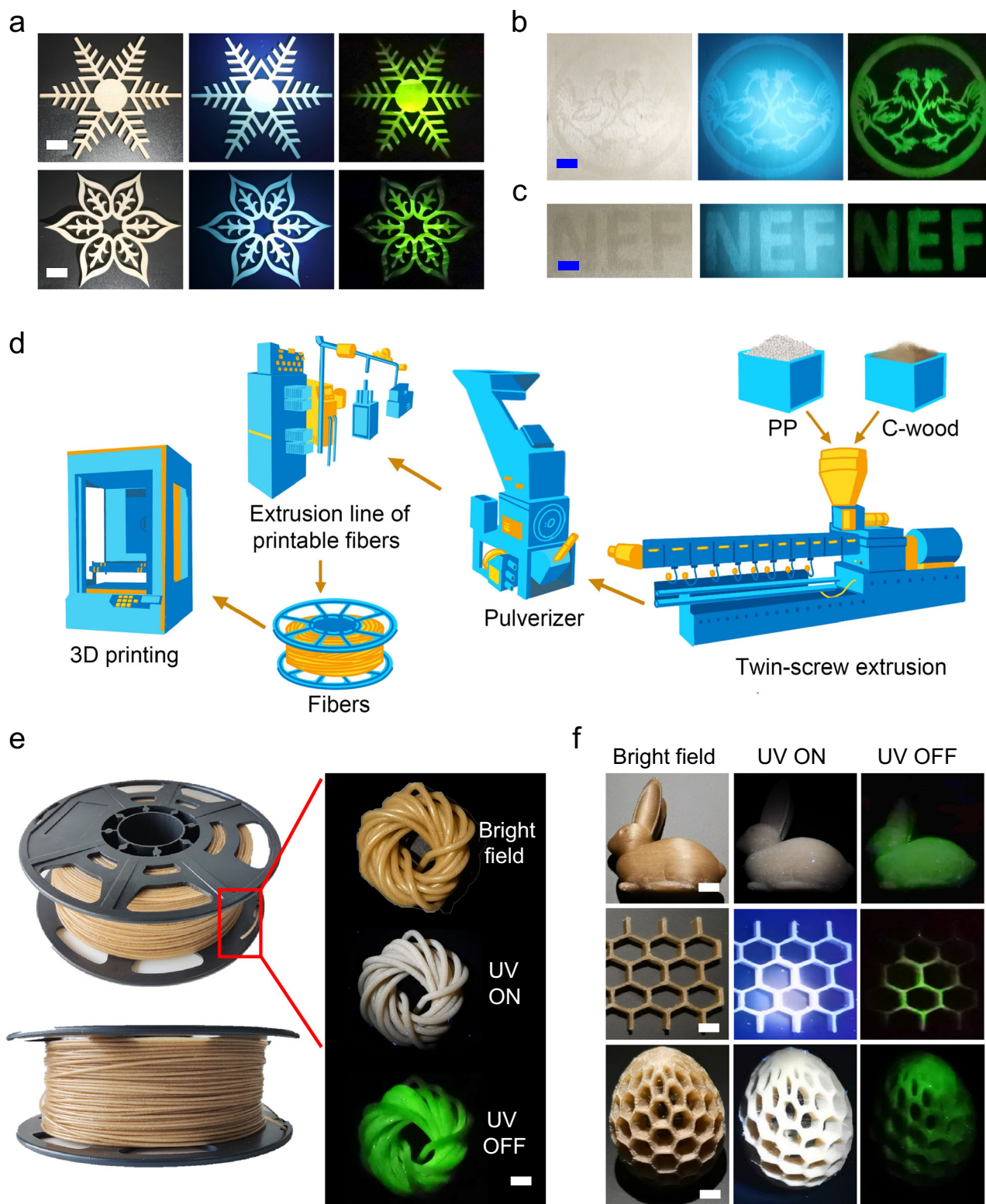
Fig. 5 | RTP emission of C-wood products. a, Photographs of C-wood sculpture before (middle) and after (right) turning off a 365 nm UV lamp; scale bar = 1 cm. **b** and **c** Photographs of C-wood pattern before (middle) and after (right) turning off a 365 nm UV lamp; scale bar = 1 cm. Afterglow images in a-c were acquired at 120 ms after switching off the UV light. **d**, Schematic illustration of fabrication of printable afterglow plastics from C-wood and polypropylene (PP). **e** Photographs of printable fiber before (middle) and after (bottom) turning off a 365 nm UV lamp; scale bar = 1 cm. **f** Photographs of printed rabbit, pinecones, and honeycomb before (middle) and after (right) turning off a 365 nm UV lamp; scale bar = 1 cm. Afterglow images in e-f were acquired at 140 ms after switching off the UV light.

materials, such as, molecular crystals, guest-host molecular systems, metal-organic frameworks and polymer composites, which are regarded as promising replacements for traditional inorganic bulk phosphorescent materials[11,71–74]. For example, the lifetime of C-wood does not show any significant improvements when compared with currently reported materials. However, C-wood does exhibit comparable lifetime with many of these materials (Fig. 6)[46,75–87]. As such an important future goal will be to enhance the lifetime of C-wood. Additionally, the
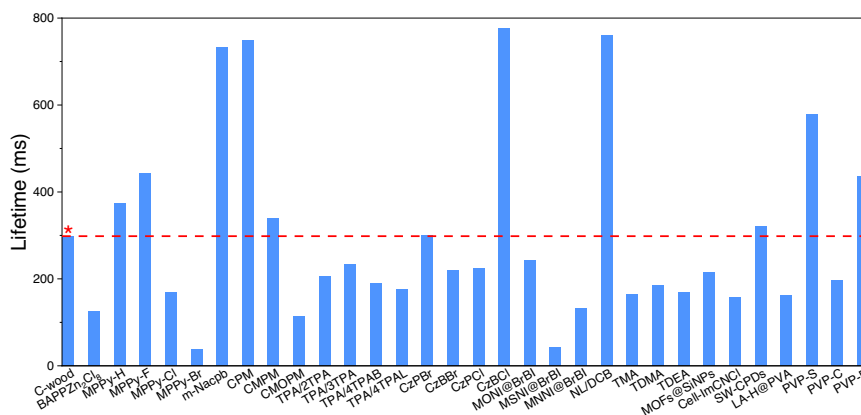
Fig. 6 | Comparison of RTP lifetime between C-wood (∗) and the reported materials. (BAPPZn₂Cl₈;[46] MPPy-H, MPPy-F, MPPy-Cl and MPPy-Br;[75] m-Nacpb;[76] CPM, CMPM and CMOPM;[77] TPA/2TPA, TPA/3TPA, TPA/4TPAB and TPA/4TPAL;[78] CzPBr, CzBBr, CzPCl and CzBCl;[79] MONI@BrBI, MSNI@BrBI and MNNI@BrBI;[80] NL/DCB;[81] TMA, TDMA and TDEA;[82] MOFs@SiNPs;[83] Cell-ImCNCl;[84] SW-CPDs;[85] LA-H@PVA;[86] PVP-S, PVP-C and PVP-B[87]).

RTP wavelength of the reported phosphorescent materials can be tuned trough targeted synthesis[88]. However, in the case of C-wood, we are limited by the naturally available structure of lignin, as such the RTP wavelength of C-wood cannot be easily modified. One possibility for future development would be to collaborate with plant physiologist to obtain modified lignin via genetic engineering[89] and grow wood with targeted RTP emission spectra after Cl⁻ modification. As such in the future it may be possible to prepare C-wood with different RTP wavelengths using modified natural wood.

Methods

Preparation of C-wood, N-wood and S-wood
The wood samples were immersed in a 1 M aqueous MgCl₂ solution (or aqueous solution of other salts that were 2 M in Cl⁻). After immersing for 2 s, the wood sample was removed from the MgCl₂ solution (or the aqueous solution of other salts) and dried at 105 °C for 60 min to give C-wood. N-wood and S-wood were obtained by replacing the MgCl₂ with 1 M aqueous Mg(NO₃)₂ or 1 M aqueous MgSO₄ solution, respectively, following the same procedure.

Preparation of lignin for 2D-HSQC NMR analysis
Choline chloride (ChCl, 2.0 g) and lactic acid (12.9 g) were mixed together and heated at 80 °C until the solid powders completely disappeared to obtain a deep eutectic solvent (DES). After that, the mixture was cooled in a desiccator. Prior to DES treatment, the wood samples were air-dried and milled to a specific size (mesh 40). After that, dry wood powders (1 g) were added to DES (10 g). The reaction mixture was maintained at 145 °C for 6 h. The mixture was then cooled down and the DES soluble fractions were separated by filtration assisted by ethanol washing (30 mL). Water (100 mL) was then added to the filtrate to precipitate the lignin. The as-obtained lignin was collected after centrifugation and freeze-dried for NMR analysis.

Klason method
Klason lignin is the insoluble residue portion after removing the ash by concentrated acid hydrolysis of the plant tissues, which is also an intuitive method for the determination of lignin content in plants. Specifically, the wood powders (1 g) were firstly washed using a mixture of benzene (67 mL) and ethanol (33 mL). After that, the wood was dried at 105 °C for 60 min. The as-dried wood was treated with concentrated sulfuric acid (72%, 15 mL) at 30 °C for 4 h. Then, water (545 mL) was added to the reaction. The reaction was further refluxed for 2 h. Finally, the reaction mixture was filtered, and as-obtained solid powders were washed by water and dried at 105 °C for 60 min to give lignin.

Preparation of printable fibers
C-wood powder was prepared by immersing basswood powder in 2 M Cl⁻ for 2 s. As-obtained C-wood powders were then dried at 105 °C for 2 h. Preparation of C-wood/PP blends: 990 g PP and 10 g C-wood powder were physically mixed. After that, the mixture was subjected to extrusion processing and pelleting at 190 °C to give C-wood/PP blends. This C-wood/PP bulk composite material was then melted and pulverized at a speed of 30 rpm. The pulverized C-wood/PP powders were further treated using a single-screw wire extruder at a temperature of 175 °C, which was subsequently wound on a wire reel. The fibers were printed into models, such as, rabbit, honeycomb and pinecones, using standard 3D printing methods.

Data availability
All relevant data are included in this article and its Supplementary Information files. Source data are provided with this paper.

References

1. Xu, S., Chen, R. F., Zheng, C. & Huang, W. Excited State Modulation for Organic Afterglow: Materials and Applications. *Adv. Mater.* **28**, 9920–9940 (2016).
2. Zhao, W. J., He, Z. K. & Tang, B. Z. Room-temperature phosphorescence from organic aggregates. *Nat. Rev. Mater.* **5**, 869–885 (2020).
3. Miao, Q. et al. Molecular afterglow imaging with bright, biodegradable polymer nanoparticles. *Nat. Biotechnol.* **35**, 1102–1110 (2017).
4. Li, Y., Gecevicius, M. & Qiu, J. R. Long persistent phosphors-from fundamentals to applications. *Chem. Soc. Rev.* **45**, 2090–2136 (2016).
5. Jia, X. et al. Photoexcitation-controlled self-recoverable molecular aggregation for flicker phosphorescence. *Proc. Natl. Acad. Sci. USA* **116**, 4816–4821 (2019).
6. Li, D., Yang, J., Fang, M., Tang, B. Z. & Li, Z. Stimulus-responsive room temperature phosphorescence materials with full-color tunability from pure organic amorphous polymers. *Sci. Adv.* **8**, eabl8392 (2022).
7. Wang, H. & Shi, H. F. Lignin rebirth enables sustainable afterglow emission. *Matter* **4**, 3087–3088 (2021).
8. Sun, Y. Q. et al. Ultralong lifetime and efficient room temperature phosphorescent carbon dots through multi-confinement structure design. *Nat. Commun.* **11**, 5591 (2020).
9. Gong, Y. X., Yang, J., Fang, M. M. & Li, Z. Room-temperature phosphorescence from metal-free polymer-based materials. *Cell Rep. Phys. Sci.* **3**, 100663 (2022).

10. Zhang, T. et al. Molecular Engineering for Metal-Free Amorphous Materials with Room-Temperature Phosphorescence. *Angew. Chem. Int. Ed.* **59**, 11206–11216 (2020).

11. Gan, N., Shi, H. F., An, Z. F. & Huang, W. Recent Advances in Polymer-Based Metal-Free Room-Temperature Phosphorescent Materials. *Adv. Funct. Mater.* **28**, 1802657 (2018).

12. Wu, Z., Nitsch, J. & Marder, T. B. Persistent Room-Temperature Phosphorescence from Purely Organic Molecules and Multi-Component Systems. *Adv. Opt. Mater.* **9**, 2100411 (2021).

13. Liang, Y.-C. et al. Water-induced ultralong room temperature phosphorescence by constructing hydrogen-bonded networks. *Nano Res.* **13**, 875–881 (2020).

14. Xiao, F. et al. Guest-host doped strategy for constructing ultralong-lifetime near-infrared organic phosphorescence materials for bioimaging. *Nat. Commun.* **13**, 186 (2022).

15. Gao, R. & Yan, D. Layered host-guest long-afterglow ultrathin nanosheets: high-efficiency phosphorescence energy transfer at 2D confined interface. *Chem. Sci.* **8**, 590–599 (2017).

16. Hamzehpoor, E. & Perepichka, D. F. Crystal Engineering of Room Temperature Phosphorescence in Organic Solids. *Angew. Chem. Int. Ed.* **59**, 9977–9981 (2020).

17. Zhang, G., Palmer, G. M., Dewhirst, M. & Fraser, C. L. A dual-emissive-materials design concept enables tumour hypoxia imaging. *Nat. Mater.* **8**, 747–751 (2009).

18. Al-Attar, H. A. & Monkman, A. P. Room-Temperature Phosphorescence From Films of Isolated Water-Soluble Conjugated Polymers in Hydrogen-Bonded Matrices. *Adv. Funct. Mater.* **22**, 3824–3832 (2012).

19. Wang, P. et al. Producing long afterglow by cellulose confinement effect: A wood-inspired design for sustainable phosphorescent materials. *Carbon* **171**, 946–952 (2021).

20. Xu, M. et al. Designing Hybrid Chiral Photonic Films with Circularly Polarized Room-Temperature Phosphorescence. *ACS Nano* **14**, 11130–11139 (2020).

21. Li, J., Wang, Y., Zhang, Y., Zheng, D. & Wang, X. Carboxylate-Induced RTP Based on Gelatin for Anticounterfeiting. *Part. Part. Syst. Charact.* **39**, 2100254 (2022).

22. Yuan, J. et al. Sustainable afterglow materials from lignin inspired by wood phosphorescence. *Cell Rep. Phys. Sci.* **2**, 100542 (2021).

23. Cai, S. et al. Ultralong Organic Phosphorescent Foams with High Mechanical Strength. *J. Am. Chem. Soc.* **143**, 16256–16263 (2021).

24. Jiang, J. et al. Tunable Photoluminescence Properties of Microcrystalline Cellulose with Gradually Changing Crystallinity and Crystal Form. *Macromol. Rapid Commun.* **42**, 2100321 (2021).

25. Wan, K. et al. Structural materials with afterglow room temperature phosphorescence activated by lignin oxidation. *Nat. Commun.* **13**, 5508 (2022).

26. Fratzl, P. Wood made denser and stronger. *Nature.* **554**, 172–173 (2018).

27. Jiang, B. et al. Lignin as a Wood-Inspired Binder Enabled Strong, Water Stable, and Biodegradable Paper for Plastic Replacement. *Adv. Funct. Mater.* **30**, 1906307 (2020).

28. Xia, Q. et al. In Situ Lignin Modification toward Photonic Wood. *Adv.Mater.* **33**, 2001588 (2021).

29. Wang, X. et al. Strong, Hydrostable, and Degradable Straws Based on Cellulose-Lignin Reinforced Composites. *Small.* **17**, 2008011 (2021).

30. Xia, Q. et al. Solar-assisted fabrication of large-scale, patternable transparent wood. *Sci. Adv.* **7**, eabd7342 (2021).

31. Ma, X. et al. When MOFs meet wood: From opportunities toward applications. *Chem* **8**, 2342–2361 (2022).

32. Sun, X., Zhang, B., Li, X., Trindle, C. O. & Zhang, G. External Heavy-Atom Effect via Orbital Interactions Revealed by Single-Crystal X-ray Diffraction. *J. Phys. Chem. A* **120**, 5791–5797 (2016).

33. Yan, Z. A., Lin, X., Sun, S., Ma, X. & Tian, H. Activating Room-Temperature Phosphorescence of Organic Luminophores via External Heavy-Atom Effect and Rigidity of Ionic Polymer Matrix. *Angew. Chem. Int. Ed.* **60**, 19735–19739 (2021).

34. Wang, J. G. et al. A facile strategy for realizing room temperature phosphorescence and single molecule white light emission. *Nat. Commun.* **9**, 2963 (2018).

35. Ma, L., Sun, S., Ding, B., Ma, X. & Tian, H. Highly Efficient Room-Temperature Phosphorescence Based on Single-Benzene Structure Molecules and Photoactivated Luminescence with Afterglow. *Adv. Funct. Mater.* **31**, 2010659 (2021).

36. Nidhankar, A. D. et al. Self-Assembled Helical Arrays for the Stabilization of the Triplet State. *Angew. Chem. Int. Ed.* **59**, 13079–13085 (2020).

37. Lucenti, E. et al. Cyclic Triimidazole Derivatives: Intriguing Examples of Multiple Emissions and Ultralong Phosphorescence at Room Temperature. *Angew. Chem. Int. Ed.* **56**, 16302–16307 (2017).

38. Wang, T. et al. Aggregation-Induced Dual-Phosphorescence from Organic Molecules for Nondoped Light-Emitting Diodes. *Adv. Mater.* **31**, 1904273 (2019).

39. Chen, C. et al. Carbazole isomers induce ultralong organic phosphorescence. *Nat. Mater.* **20**, 175–180 (2021).

40. Tian, Z. et al. Multilevel Data Encryption Using Thermal-Treatment Controlled Room Temperature Phosphorescence of Carbon Dot/Polyvinylalcohol Composites. *Adv. Sci.* **5**, 1800795 (2018).

41. Cai, S. et al. Enabling long-lived organic room temperature phosphorescence in polymers by subunit interlocking. *Nat. Commun.* **10**, 4247 (2019).

42. Zhai, Y. et al. Carbon dots confined in 3D polymer network: Producing robust room temperature phosphorescence with tunable lifetimes. *Chin. Chem. Lett.* **33**, 783–787 (2022).

43. Jia, C. et al. From Wood to Textiles: Top-Down Assembly of Aligned Cellulose Nanofibers. *Adv. Mater.* **30**, e1801347 (2018).

44. Liang, Y.-C. et al. Phosphorescent Carbon-Nanodots-Assisted Förster Resonant Energy Transfer for Achieving Red Afterglow in an Aqueous Solution. *ACS Nano* **15**, 16242–16254 (2021).

45. Zheng, Y. et al. Full-Color Long-Lived Room Temperature Phosphorescence in Aqueous Environment. *Small* **18**, 2201223 (2022).

46. Wei, J.-H., Ou, W.-T., Luo, J.-B. & Kuang, D.-B. Zero-Dimensional Zn-Based Halides with Ultra-Long Room-Temperature Phosphorescence for Time-Resolved Anti-Counterfeiting. *Angew. Chem. Int. Ed.* **134**, e202207985 (2022).

47. Doroodmand, M. M. & Askari, M. Synthesis of a novel nitrogen-doped carbon dot by microwave-assisted carbonization method and its applications as selective probes for optical pH (acidity) sensing in aqueous/nonaqueous media, determination of nitrate/nitrite, and optical recognition of NOX gas. *Anal. Chim. Acta.* **968**, 74–84 (2017).

48. Karali, K. K., Sygellou, L. & Stalikas, C. D. Highly fluorescent N-doped carbon nanodots as an effective multi-probe quenching system for the determination of nitrite, nitrate and ferric ions in food matrices. *Talanta* **189**, 480–488 (2018).

49. Li, Q. et al. Induction of long-lived room temperature phosphorescence of carbon dots by water in hydrogen-bonded matrices. *Nat. Commun.* **9**, 734 (2018).

50. Li, D. et al. Completely aqueous processable stimulus responsive organic room temperature phosphorescence materials with tunable afterglow color. *Nat. Commun.* **13**, 347 (2022).

51. Zhu, L. et al. Transparent Bioplastics from Super-Low Lignin Wood with Abundant Hydrophobic Cellulose Crystals. *ACS Sustainable Chem. Eng.* **10**, 13775–13785 (2022).

52. Zhang, X., Li, L. & Xu, F. Chemical Characteristics of Wood Cell Wall with an Emphasis on Ultrastructure: A Mini-Review. *Forests* **13**, 439 (2022).

53. Yang, Q. et al. Rechargeable Aqueous Mn-Metal Battery Enabled by Inorganic-Organic Interfaces. *Angew. Chem. Int. Ed.* **61**, e202206471 (2022).

54. Shi, Z. et al. Bioapplications of small molecule Aza-BODIPY: from rational structural design to in vivo investigations. *Chem. Soc. Rev.* **49**, 7533–7567 (2020).

55. Xiao, Y.-F. et al. Achieving high singlet-oxygen generation by applying the heavy-atom effect to thermally activated delayed fluorescent materials. *Chem. Commun.* **57**, 4902–4905 (2021).

56. Galland, M. et al. A "Multi-Heavy-Atom" Approach toward Biphotonic Photosensitizers with Improved Singlet-Oxygen Generation Properties. *Chem. Eur. J.* **25**, 9026–9034 (2019).

57. Wan, Q. et al. Molecular Engineering to Boost AIE-Active Free Radical Photogenerators and Enable High-Performance Photodynamic Therapy under Hypoxia. *Adv. Funct. Mater.* **30**, 2002057 (2020).

58. Jia, C. et al. Rich Mesostructures Derived from Natural Woods for Solar Steam Generation. *Joule.* **1**, 588–599 (2017).

59. He, F. et al. A simple, mild and versatile method for preparation of photothermal woods toward highly efficient solar steam generation. *Nano Energy.* **71**, 104650 (2020).

60. Garemark, J. et al. Advancing Hydrovoltaic Energy Harvesting from Wood through Cell Wall Nanoengineering. *Adv. Funct. Mater.* **33**, 2208933 (2023).

61. Montanari, C., Ogawa, Y., Olsen, P. & Berglund, L. A. High Performance, Fully Bio-Based, and Optically Transparent Wood Biocomposites. *Adv. Sci.* **8**, 2100559 (2021).

62. Santos, R. B., Capanema, E. A., Balakshin, M. Y., Chang, H.-M. & Jameel, H. Lignin Structural Variation in Hardwood Species. *J. Agric. Food Chem.* **60**, 4923–4930 (2012).

63. Ralph, J., Lapierre, C. & Boerjan, W. Lignin structure and its engineering. *Curr. Opin. Biotechnol.* **56**, 240–249 (2019).

64. Xue, Y. et al. Aggregation-induced emission: the origin of lignin fluorescence. *Polym. Chem.* **7**, 3502–3508 (2016).

65. Ma, Z. et al. Seeking Brightness from Nature: J-Aggregation-Induced Emission in Cellulolytic Enzyme Lignin Nanoparticles. *ACS Sustain.Chem. Eng.* **6**, 3169–3175 (2018).

66. Chen H. Lignocellulose Biorefinery Feedstock Engineering. 37–86 (2015).

67. Alvarez-Vasco, C. et al. Unique low-molecular-weight lignin with high purity extracted from wood by deep eutectic solvents (DES): a source of lignin for valorization. *Green Chem.* **18**, 5133–5141 (2016).

68. Li, Q. et al. Study on preparation and properties of energy-storing self-luminous plastics. *Energy Rep.* **7**, 559–565 (2021).

69. Zhang, Y. et al. Large-Area, Flexible, Transparent, and Long-Lived Polymer-Based Phosphorescence Films. *J. Am. Chem. Soc.* **143**, 13675–13685 (2021).

70. Yang, X. & Berglund, L. A. Structural and Ecofriendly Holocellulose Materials from Wood: Microscale Fibers and Nanoscale Fibrils. *Adv.Mater.* **33**, 2001118 (2021).

71. Shi, H. et al. Ultralong Organic Phosphorescence: From Material Design to Applications. *Acc. Chem. Res.* **55**, 3445–3459 (2022).

72. Ma, X., Wang, J. & Tian, H. Assembling-Induced Emission: An Efficient Approach for Amorphous Metal-Free Organic Emitting Materials with Room Temperature Phosphorescence. *Acc. Chem. Res.* **52**, 738–748 (2019).

73. Hirata, S. Recent Advances in Materials with Room-Temperature Phosphorescence: Photophysics for Triplet Exciton Stabilization. *Adv. Optical Mater.* **5**, 1700116 (2017).

74. Gao, R., Kodaimati, M. S. & Yan, D. Recent advances in persistent luminescence based on molecular hybrid materials. *Chem. Soc. Rev.* **50**, 5564–5589 (2021).

75. Wang, M. et al. Excitation-dependent organic phosphors exhibiting different luminescence colors for information anti-counterfeiting. *Chem. Eng. J.* **429**, 132288 (2022).

76. Nie, F., Zhou, B. & Yan, D. Ultralong room temperature phosphorescence and reversible mechanochromic luminescence in ionic crystals with structural isomerism. *Chem. Eng. J.* **453**, 139806 (2023).

77. Xie, Y. et al. How the Molecular Packing Affects the Room Temperature Phosphorescence in Pure Organic Compounds: Ingenious Molecular Design, Detailed Crystal Analysis, and Rational Theoretical Calculations. *Adv. Mater.* **29**, 1606829 (2017).

78. Yang, J. et al. Achieving Efficient Phosphorescence and Mechanoluminescence in Organic Host-Guest System by Energy Transfer. *Adv. Funct. Mater.* **31**, 2108072 (2021).

79. Yin, Z. et al. Molecular Engineering through Control of Structural Deformation for Highly Efficient Ultralong Organic Phosphorescence. *Angew. Chem. Int. Ed.* **60**, 2058–2063 (2021).

80. Chen, B. et al. An Organic Host-Guest System Producing Room-Temperature Phosphorescence at the Parts-Per-Billion Level. *Angew. Chem. Int. Ed.* **60**, 16970–16973 (2021).

81. Zhang, X. et al. Highly efficient and persistent room temperature phosphorescence from cluster exciton enables ultrasensitive off-on VOC sensing. *Matter* **5**, 3499–3512 (2022).

82. Liu, H. et al. Highly Efficient Blue Phosphorescence from Pillar-Layer MOFs by Ligand Functionalization. *Adv. Mater.* **34**, 2107612 (2022).

83. Wang, J. et al. Multi-modal anti-counterfeiting and encryption enabled through silicon-based materials featuring pH-responsive fluorescence and room-temperature phosphorescence. *Nano Res.* **13**, 1614–1619 (2020).

84. Zhang, X. et al. Ultralong phosphorescence cellulose with excellent anti-bacterial, water-resistant and ease-to-process performance. *Nat. Commun.* **13**, 1117 (2022).

85. Wang, Z. et al. Gram-Scale Synthesis of 41% Efficient Single-Component White-Light-Emissive Carbonized Polymer Dots with Hybrid Fluorescence/Phosphorescence for White Light-Emitting Diodes. *Adv. Sci.* **7**, 1902688 (2020).

86. Liu, R., Jiang, T., Liu, D. & Ma, X. A facile and green strategy to obtain organic room-temperature phosphorescence from natural lignin. *Sci. China Chem.* **65**, 1100–1104 (2022).

87. Wang, H. et al. Amorphous Ionic Polymers with Color-Tunable Ultralong Organic Phosphorescence. *Angew. Chem. Int. Ed.* **58**, 18776–18782 (2019).

88. Dou, X. et al. Color-Tunable, Excitation-Dependent, and Time-Dependent Afterglows from Pure Organic Amorphous Polymers. *Adv. Mater.* **32**, 2004768 (2020).

89. Pazhany, A. S. & Henry, R. J. Genetic Modification of Biomass to Alter Lignin Content and Structure. *Ind. Eng. Chem. Res.* **58**, 16190–16203 (2019).

Acknowledgements

Author contributions

Conceptualization: Z.C., S.L., T.D.J., J.L.S.; Methodology: Y.Z.; Investigation: Y.Z.; Visualization: Y.Z., S.L., J.L., S.Liu; Supervision: Z.C., S.L., T.D.J., J.L.S.; Writing-original draft: All authors; Writing-review & editing: All authors.

Competing interests

T.D.J acts as a scientific consultant for Z. C. at Northeast Forestry University. All other authors declare no competing interests.

Additional information

Supplementary information The online version contains supplementary material available at https://doi.org/10.1038/s41467-023-37762-9.

Correspondence and requests for materials should be addressed to Shujun Li, Tony D. James, Jonathan L. Sessler or Zhijun Chen.

Peer review information *Nature Communications* thanks Chaolong Yang and the other, anonymous, reviewer(s) for their contribution to the peer review of this work.

Reprints and permissions information is available at http://www.nature.com/reprints

Publisher's note Springer Nature remains neutral with regard to jurisdictional claims in published maps and institutional affiliations.